

Structural and Antibacterial Properties of PVDF doped $Mn_xZn_{1-x}Fe_2O_4$ Nano-ferrites

Nawras Kareem Ali^a, Zainab Raheem Muslim^{b*}

^{a,b*}Physics Department, College of science, University of Baghdad, Baghdad, Iraq.

*Corresponding author E-mail: nouras.kareem1104a@sc.uobaghdad.edu.iq

Abstract

Manganese-Zinc Ferrite ($Mn_xZn_{1-x}Fe_2O_4$) powder was prepared using the "sol-gel" technique. Structure and antibacterial properties of the sample were investigated by XRD, AFM, EDX, and FE-SEM. X-ray diffraction (XRD) determined that $Mn_xZn_{1-x}Fe_2O_4$ has a cubic structure. The atomic force microscopy (AFM) determined that the average diameter of Manganese-Zinc Ferrite is (55.35nm), indicating that the sample has a nano-structure dimension. Energy dispersive X-ray (EDX), was conducted to assess the surface morphology and elemental compositions of Manganese-Zinc Ferrite. FE-SEM was used to look at the shape of the surface. The microphotograph showed that the shape was homogeneously spherical. Antibacterial properties results for PVDF, pure $Mn_xZn_{1-x}Fe_2O_4$ and PVDF doped different ratio $Mn_xZn_{1-x}Fe_2O_4$ and add a constant amount of activated carbon (PVDF: $Mn_xZn_{1-x}Fe_2O_4$ /AC) to study the biological activity for two types of bacteria positive S-aurous and negative E-coil the result showed the nano-ferrite has good activity for both type and the diameter for inhibition zones was ranged (25-17) mm.

Key Words

$Mn_xZn_{1-x}Fe_2O_4$, XRD, AFM, EDX, FE-SEM, Antibacterial properties.

Introduction

Recently, there has been a great deal of interest in studying spinel ferrite nanoparticles due to their unique physical, electrical, electronic, catalytic, and magnetic properties as well as their uses in technology. Most spinel ferrites belong to the $Fd3m$ space group, however some spinels exhibit lower symmetry [1]. Spinel ferrites are homogenous materials consisting primarily of iron and have a general chemical formula of MFe_2O_4 , in which M^{2+} and Fe^{3+} respectively reside in tetrahedral and octahedral metallic cation spots of the lattice [2]. The minuscule dimension of spinel ferrite makes them an ideal candidate in a broad spectrum of biological applications, including their use as contrast agents in magnetic resonance imaging (MRI) [3], targeted drug delivery, and magnetic hyperthermia [4]. Among spinel ferrites, have gained attention in

various biomedical applications due to their bio-friendly character, lower toxicity than other metal ferrites, chemical stability, easy and reproducible synthesis, low saturation magnetization, and photo-induced catalytic reactant properties [5, 6].

Manganese-Zinc Ferrite ($Mn_xZn_{1-x}Fe_2O_4$) have spinel structure [7]. The unit cell of spinel ferrite is FCC with eight formula units per unit cell having 64 tetrahedral sites surrounded by four oxygen atoms and 32 octahedral sites, surrounded by six oxygen atoms [8]. In MnZn spinel ferrite lattice, Zn ions are on the tetrahedral sites while Fe and Mn ions occupy both tetrahedral and octahedral sites [9]. MnZn ferrites are preferred due to high permeability, saturation induction, low power losses and high magnetic induction [10]. MnZn ferrites are of great interest due to their wide range of applications such as

hyperthermia applications [11], power applications [12], magnetic fluid, high frequency power supply [13], memory storage devices, TV sets, biomedicines, magnetic resonance, and catalysis [14].

Polyvinylidene fluoride (PVDF) is semi-crystalline polymorphs due to the presence of elemental fluorine (F) of the starting molecular base. PVDF normally has a crystallinity of roughly 50% and, depending on the processing parameters, can appear in four different crystalline phases designated as α , β , γ and δ . PVDF has a glass transition temperature of roughly and crystalline. Poly (vinylidene fluoride) PVDF and its copolymer are the polymer with heights dielectric constants, including chemical agent resistance, lightness, pyroelectric, piezoelectric and ferroelectric. PVDF could form at least five different crystalline phases among which the α and β phases are the most common, the most stable polymorph of PVDF is the α -form [15-16].

There are various techniques for producing ferrite nanoparticles, such as the combustion, forced hydrolysis, redox process, co-precipitation, hydrothermal, spray drying, sol-gel, solid state reaction, sonochemical, thermal decomposition method, and electrochemical [17]. The sol-gel method is an environmentally friendly and cost-effective method for synthesizing magnetic ferrite particles [18]. The advantages of sol-Gel technique include its relative simplicity, low cost ability to be performed at a low temperature without specialized equipment, and ability to achieve a Small particle size distribution [19]. In this study, the structure and Antibacterial of Mn-doped Zn ferrite nano ferrites were synthesized using the

chemical "sol-gel" technique, followed by grinding and calcinations at 700°C. Study the biological activity for two types of bacteria positive S-aurous and negative E-coil.

Experimental Procedure

1. Preparation of Manganese-Zinc Ferrite ($Mn_xZn_{1-x}Fe_2O_4$)

$Mn_{0.5}Zn_{0.5}Fe_2O_4$ composite was prepared using the Sol-gel technique. The materials used to prepare $Zn_{0.5}Mn_{0.5}Fe_2O_4$, nitrates (Zinc, Manganese and iron) were mixed with deionized water (30ml), and then citric acid added into solution (1:1:1:3). The mixture was heated under stirring at 80 °C for five hours, which made the mixture denser and formed the gel. The gel was oven-dried at 150 degrees Celsius for six hours. The powder was calcined at 700 °C for five hours in air to obtain the pure crystalline stage. Finally, the sample would be further analyzed using XRD, AFM, EDX, and FE-SEM.

2. Preparation of Bacteria

The Staphylococcus aureus (Staph.) and Escherichia coli (E. coli) microorganisms by disk diffusion method in accordance with the procedure described by Hwang and Ma This Method is a mean of measuring the effects of an antimicrobial agent on bacteria growth in a culture. Muller-Hinton Agar (MHA) powder was used as a culture medium for bacteria growth. To prepare the culture medium, 19 g of agar was dissolved into 500 ml of distilled water, and then a transparent brown solvent was achieved via boiling the solution. MHA medium (15 ml) was sterilized at 120°C for about 1 hour in autoclave cooled to room temperature and then poured into sterilized petri dishes

(10mm). After cooling over 24 hours, the bacteria are swabbed uniformly across the culture plate. Filter-paper disks were placed on the surface of agar. To evaluate the antibacterial activity, 100µl of each of the samples was dropped moderately on disks' surface using a sampler. If the samples are effective against the bacteria at a certain concentration, then no colonies would grow and the concentration in agar is greater than or equal to the effective concentration. This region is called inhibition zone. The size of inhibition zone measures the efficacy of sample. A more effective sample produces a larger clear area around the disk. All tests were done under laminar flow hood. Finally, all petri dishes containing bacteria and antibacterial reagents were incubated at 37°C for 24 h. At the end of incubation period, the diameters of inhibition zones formed around disks, were determined and presented in mm. The results concerning antibacterial activity were expressed as strong activity diameters of inhibition zone is (>13 mm), moderate activity (6 – 12 mm), weak activity (5 mm) or no activity (inhibition zone < 5 mm).

Results and Discussion

1. X-ray Diffraction Analysis

The X-ray diffraction spectra for the Manganese-Zinc Ferrite ($Mn_xZn_{1-x}Fe_2O_4$) synthesized using the sol-gel technique are shown in Figure 1. X-ray spectra indicate cubic structure $Mn_xZn_{1-x}Fe_2O_4$ with card (JCPDS NO. 96-901-3530), and the second phase Hematite Fe_2O_3 has cubic structure with card (JCPDS NO. 96-900-9783). The main peaks at 18.2184, 29.9713, 35.2874, 36.8678, 42.9023, 53.2471, 56.7529, 62.3276, 70.7759, and 73.5920 correspond to (111), (220), (222), (311), (400), (422), (511), (440), (620) and (533) indicates the formation of pure $Mn_xZn_{1-x}Fe_2O_4$, some extra secondary peaks (secondary phases of Hematite Fe_2O_3) can be seen adjacent to the peak features. This may be due to the presence of the impurity process. Formation of impurity phase of hematite during calcination at 700°C could be due to hematite is thermally stable at a high annealing temperature. This agrees with the result obtained by [20]. And table1 explained the structural properties (index plan, FWHM, and grain size).

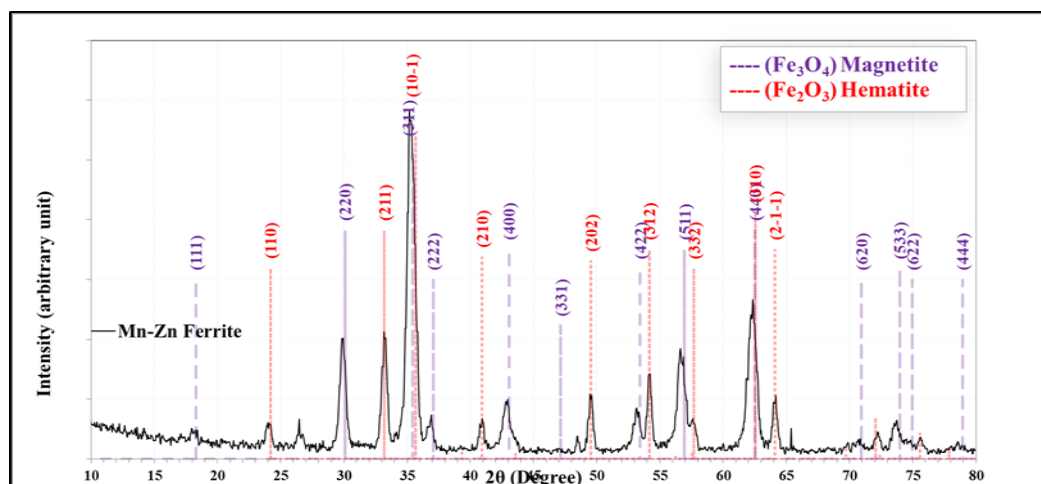


Figure 1: X-ray diffraction spectra of $Mn_xZn_{1-x}Fe_2O_4$

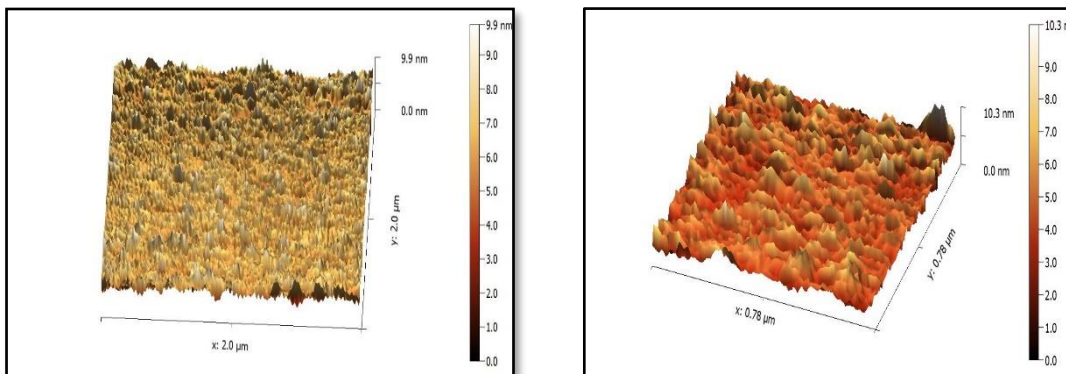
Table 1: The structural properties of Mn_xZn_{1-x}Fe₂O₄ powder

2. AFM and EDX for Mn_xZn_{1-x}Fe₂O₄

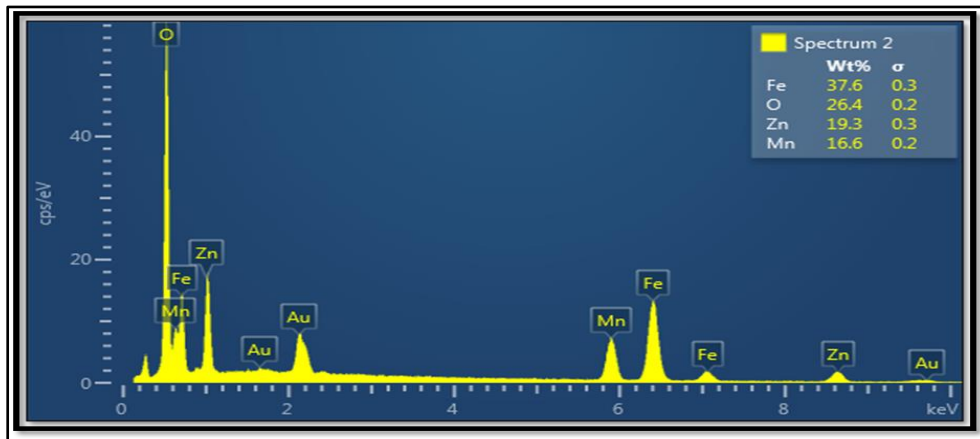
The atomic force microscope (AFM) micrograph of Mn_xZn_{1-x}Fe₂O₄ is appeared in Fig. 2. It can be seen in Fig. 2 (a,b) that the sample has a consistent spherical shape and a uniform grain distribution over the surface. The average diameter was determined to be 55.35 nm, indicating that the sample has a nanostructure. Moreover, in order to characterize the elemental composition on the surface of Mn_xZn_{1-x}Fe₂O₄ particle, the corresponding energy dispersive X-ray (EDX) spectrum were analyzed in Figure (3)

shows the peaks of Fe, Mn, Zn and O elements for Mn_xZn_{1-x}Fe₂O₄ sample. The result confirms the presence of the components Fe, Zn and Mn. The highest intensity of Fe may be seen in the spectrum of the sample. A small peak was appeared at 2.1 KeV which indicated that presence of Au (gold) peak, which has been used as a sputter coating, while preparing the sample. The atomic ratio of Fe: Zn: Mn: O was found to be (23.04:10.10:10.34:56.52) for Zn_{1-x}Mn_xFe₂O₄.

Figure 2: AFM micrograph for Mn_xZn_{1-x}Fe₂O₄ were a) 2D, b) 3D



Sample	2θ (Deg.)	FWHM (Deg.)	d _{hkl} Exp. (Å)	G.S (nm)	hkl	Phase	card No.
Mn-Zn Ferrite	18.2759	0.6896	4.8504	11.7	(111)	Magnetite	96-901-3530
	24.0517	0.5747	3.6971	14.1	(110)	Hematite	96-900-9783
	29.8563	0.6034	2.9902	13.6	(220)	Magnetite	96-901-3530
	33.2184	0.4885	2.6948	17.0	(211)	Hematite	96-900-9783
	35.2299	0.6896	2.5454	12.1	(311)	Magnetite	96-901-3530
	36.9253	0.4310	2.4324	19.4	(220)	Magnetite	96-901-3530
	40.9195	0.4886	2.2037	17.4	(210)	Hematite	96-900-9783
	42.8448	0.5460	2.1090	15.6	(400)	Magnetite	96-901-3530
	49.5690	0.4310	1.8375	20.3	(202)	Hematite	96-900-9783
	53.1609	0.4885	1.7215	18.2	(422)	Magnetite	96-901-3530
	54.1954	0.4311	1.6911	20.7	(312)	Hematite	96-900-9783
	56.6379	0.6322	1.6238	14.3	(511)	Magnetite	96-901-3530
	57.6437	0.4885	1.5978	18.6	(332)	Hematite	96-900-9783
	62.3276	0.7758	1.4885	12.0	(440)	Magnetite	96-901-3530
	64.1379	0.4023	1.4508	23.3	(2-1-1)	Hematite	96-900-9783
70.7759	0.5173	1.3301	18.8	(620)	Magnetite	96-901-3530	
73.7069	0.6610	1.2843	15.0	(533)	Magnetite	96-901-3530	

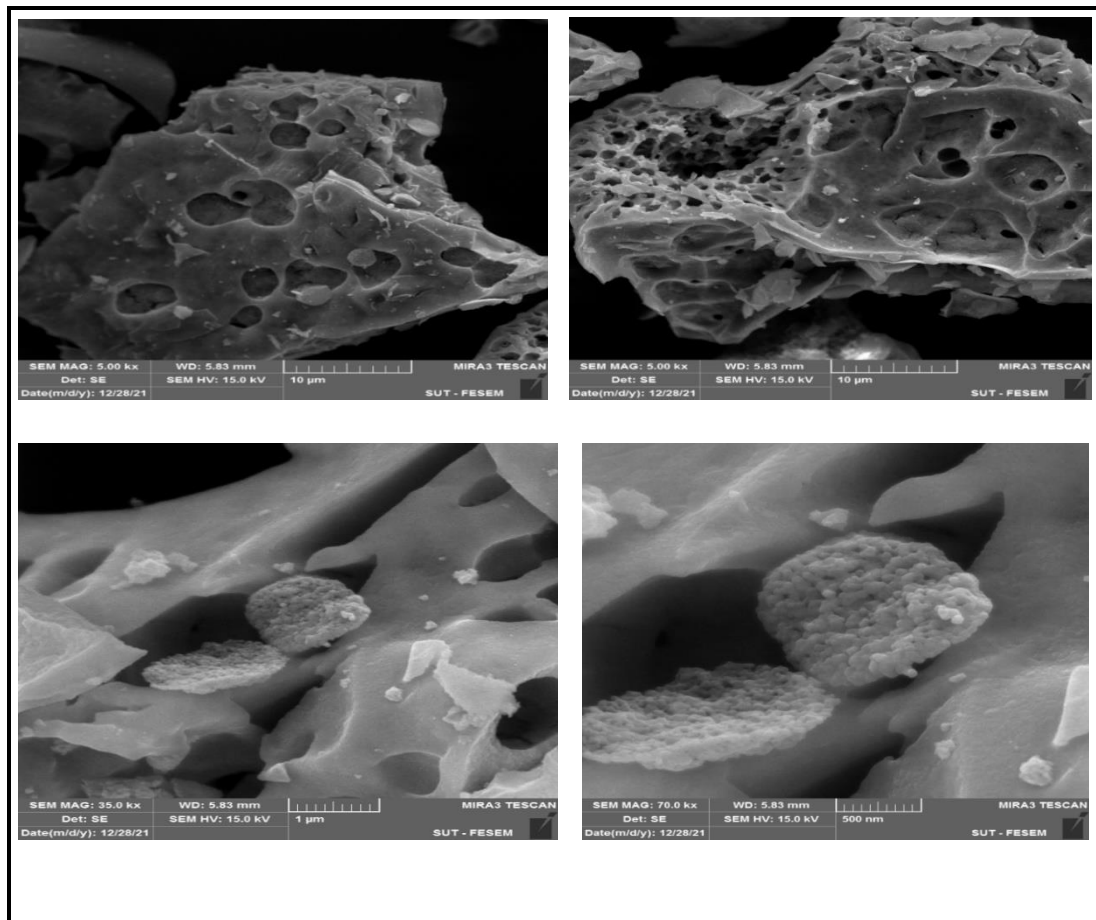
Figure 3: EDX for $Mn_xZn_{1-x}Fe_2O_4$ 

3. Field Emission Scanning Electron Microscope (FE-SEM)

Field emission scanning electron microscopy (FE-SEM) of the manganese-zinc ferrite ($Mn_xZn_{1-x}Fe_2O_4$) sample prepared by the sol-gel process. High-resolution FE-SEM images of the manganese-zinc ferrite sample calcined at 700 degrees Celsius for five hours are shown in Figure 4; the FE-SEM images indicate that the as-prepared sample consisted

of well-crystallized homogenous particles, most of which are spherical in shape and smooth on the surface. It is also worth noting that faceted crystals can be seen, and the diameter of the manganese-zinc ferrite ($Mn_xZn_{1-x}Fe_2O_4$) particles is calculated to be in the range D1 (58.34-75.83 nm) from Figure

4.



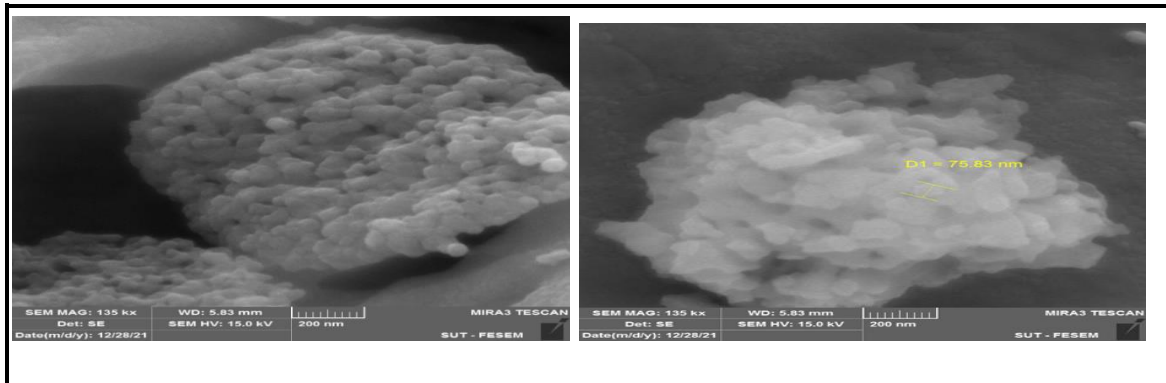


Figure 4: FE-SEM images of $Mn_xZn_{1-x}Fe_2O_4$

4. Antibacterial activity Properties

4. $Mn_xZn_{1-x}Fe_2O_4$ and pure PVDF 1 Antibacterial activity for

The antibacterial activity for samples was conducted using Gram-positive (*S. aureus*) and Gram-negative (*E. coli*) as pathogens. The results are shown in Fig.(5) and Fig (6) for pure PVDF, and Manganese-Zinc ferrite samples showed positive antibacterial activity against *S. aureus* with an inhibition zone of 20 and 21 mm in respectively, whereas for *E. coli* were 20 and 28 mm, respectively. The bacterial activity of ferrite depends on the size, morphology, chemical molecule diffusion ability, and the discharge

of metal ions. In addition, the surface area is crucial in the elevated and promising activity of $Mn_xZn_{1-x}Fe_2O_4$ nanoparticles against all the tested pathogenic microbes. There are many reasonable mechanisms for the antimicrobial action of $Mn_xZn_{1-x}Fe_2O_4$ nanoparticles, including radical groups generated through the redox reactions during the photocatalytic process attack the bacteria's cell membrane components and inhibit the growth of these microorganisms.

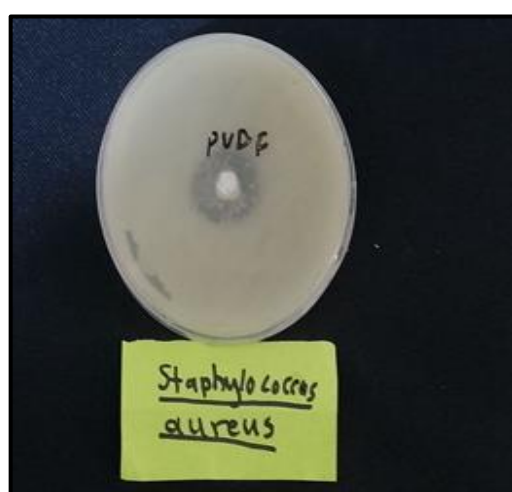


Figure 5: A schematic illustration of created inhibition zones for E.coli of PVDF **Figure 6:**
A schematic illustration of created inhibition zones for E.coli and S.aureus of $Mn_xZn_{1-x}Fe_2O_4$

4. 2Antibacterial activity of PVDF doped $Mn_xZn_{1-x}Fe_2O_4$ ferrites

The antibacterial activity of manganese-Zinc ferrite of (PVDF: Mn-ZnF /AC), with different ratio (1%, 2%, and 3%) wt, was performed on gram-positive (*Staphylococcus aureus*) and gram-negative (*Escherichia coli*) bacterial strains. Figure 7 shows the samples have significant antibacterial activity against *Escherichia coli* bacteria with an inhibition area of 18 mm, 19mm and 21 mm (Figure 7a). This result was higher compared to *Staphylococcus aureus* bacteria with an inhibition area of 17mm, 18mm, and 20 mm (Figure 7b). The bacterial activity of manganese-Zinc ferrite depends on the size, morphology, surface area, chemical molecule diffusion ability and also the discharge of metal ions. The antibacterial ability of (PVDF/mn-Zn/AC 3%) samples was better because of the smaller particle size of (PVDF/mn-Zn/AC 3%) so that it easily covers and penetrates the cell walls

of bacteria. Besides, *Staphylococcus aureus* bacteria are more easily inhibited than *Escherichia coli* due to this bacterial has a structure with high peptidoglycan content so it is difficult to penetrate the cell walls of bacteria and inhibit its growth. Synthesized and tested the manganese ferrite antibacterial activity against *Staphylococcus aureus* and *Escherichia coli* but showed no antibacterial activity at all due to the small outer surface of the ferrite material [21]. Bactericidal activity would differ depending on the cell wall nature of bacteria. The cell wall of Gram-positive bacteria is wider than the cell the Gram-negative bacteria [22]. The proposed mechanism of antibacterial activity of the photocatalytic materials are described as followed. When coming in contact with microbes, they will affect the bacterial cell membrane and start to influence the metabolism of the cells.



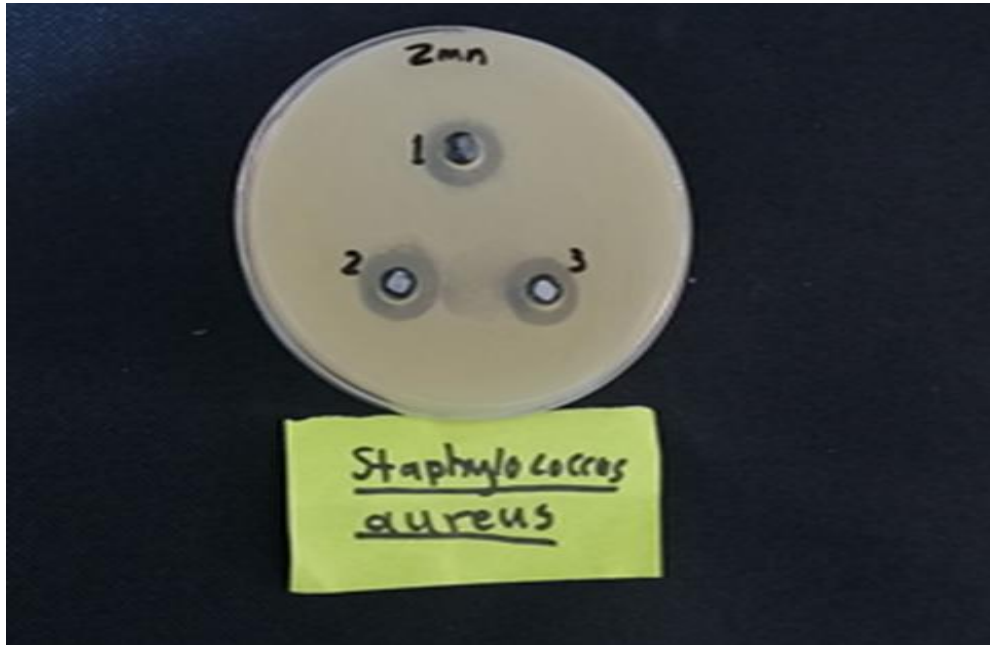


Figure 7 a: A schematic illustration of created inhibition zones for E.coli of (PVDF/Mn-ZnF/AC)



Figure 7 b: A schematic illustration of created inhibition zones for S.aurous of (PVDF/Mn-ZnF/AC)

Conclusion

The structural and properties of PVDF doping Manganese-Zinc Ferrite ($Mn_xZn_{1-x}Fe_2O_4$) Nano-ferrites that were prepared

using the Sol-Gel technique. XRD results reveal the sample a cubic structure. SEM and AFM analysis were used to examine the morphology and average diameter of

Manganese -Zinc Ferrite. An (EDX) a spectrum reveals the presence of transition metals (Mn, Zn, Fe, and O). The PVDF doping Manganese-Zinc Ferrite was proved biological activity for two types of bacteria positive and negative and was much active for E.coli because the S.aurous has hard.

References

1. Uma Shankar Sharma a and Rashmi Shah, Investigation of Effect of Mn doping in Magnetic Properties of $ZnFe_2O_4$.AIP conference ,proceedings, 2020,Vol.6,pp.1-020117.
2. Issa B, Obadiah I, Alibis B, et al. *Magnetic nanoparticles: Surface effects and properties related to biomedicine applications*. 2013, Vol.14, pp.21266-21305.
3. Covaliu C.I., Berger D., Matei C., Diamandescu L., Vasile E., Cristea C., Ionita V., Iovu H. *Magnetic nanoparticles coated with polysaccharide polymers for potential biomedical applications*. J. Nanoparticle Res. 2011; Vol.13, pp.6169–6180.
4. Nawras Kareem Ali and Zainab Raheem Muslimb, *Preparation and Characterization of Spinal Zinc Ferrite $ZnFe_2O_4$ Using the Sol-gel technique*. Journal TELECOMMUNICATIONS, 2022, Vol.21, pp.5327-5335.
5. Patel J., Parekh K., Upadhyay R.V. *Performance of Mn-Zn ferrite magnetic fluid in a prototype distribution transformer under varying loading conditions*. Int. J. Therm. Sci. 2017; Vol.114, pp.64–71.
6. Welch R.G., Neamtu J., Rogalski M.S., Palmer S.B. *Polycrystalline MnZn ferrite films prepared by pulsed laser deposition*. Mater. Lett. 1996; Vol. 29, pp.199–203.
7. Sanatombi S., Sumitra S., Ibetombi S. *Influence of sintering on the structural, electrical, and magnetic properties of Li–Ni–Mn–Zn ferrite synthesized by citrate precursor method*. Iran. J. Sci. Technol. Trans. A-Science. 2018, Vol.42, pp.2397–2406.
8. Reddy D.H.K., Yun Y.S. *Spinel ferrite magnetic adsorbents: alternative future materials for water purification? Coord. Chem. Rev.* 2016, Vol.315, pp.90–111.
9. Tsakaloudi V., Papazoglou E., Zaspalis V.T. *Microwave firing of MnZn-ferrites*. Mater. Sci. Eng. B: Solid-State Materials for Advanced Technology. 2004, Vol.106, pp.289–294.
10. Li M., Fang H., Li H., Zhao Y., Li T., Pang H., Tang J., Liu X. *Synthesis and characterization of MnZn ferrite nanoparticles with improved saturation magnetization*. J. Supermom. Nov. Magnetism. 2017, Vol.30, pp.2275–2281.
11. Parekh K., Upadhyay R.V., Belova L., Rao K.V. *Ternary monodispersed $Mn_{0.5}Zn_{0.5}Fe_2O_4$ ferrite nanoparticles: preparation and magnetic characterization*. Nanotechnology. 2006; Vol.17, pp.5970–5975.
12. Hua F., Yin C., Zhang H., Suo Q., Wang X., Peng H. *Direct preparation of the Nanocrystalline MnZn ferrites by using oxalate as precipitant*. J. Mater. Sci. Chem. Eng. 2015, pp.23–

29. *of nanocrystalline zinc–ferrite as material for micro waves absorption by sol-gel methods.* Journal Science and Technology, 2017, 10(21), pp. 1–6.
13. Verma A., Alam M.I., Chatterjee R., Goel T.C., Mendiratta R.G. *Development of a new soft ferrite core for power applications.* J. Mango. Mango Mater. 2006, Vol.300, pp.500–505.
14. Latorre-Esteves M., Cortés A., Torres-Lugo M., Rinaldi C. *Synthesis and characterization of carboxymethyl dextran-coated Mn/Zn ferrite for biomedical applications.* J. Mango. Mango Mater. 2009, Vol.321, pp.3061–3066.
15. Ruqaya Fouad and Zaniab Raheem, *Structural and Electrical properties of PVDF doping lithium Iron Oxide nano-composites.* Journal of physics: Conference series, 2020, pp. 1–10.
16. S. El-Sayed, T. A. Abdel-Baset, and A. Hassen, “*Dielectric properties of PVDF thin films doped with 3 wt. % of R Cl 3 (R = Gd or Er),*” AIP Adv., 2014, vol. 4, no. 3, pp. 0–15.
17. Ahmed M.Hammed and Zainab Raheem Muslim., *Effect of addition on the structure and magnetic properties of $Ni_{1-x}Al_xFe_2O_4$ prepared via sol-gel method.* Journal Materials science and Engineering, 2020,928, pp.109681.
18. H.T John, Fraih, and A.J., *Preparation*
19. Samah Abd Kadhum and Zainab Raheem Muslim., *Synthesis and characterization of Li_2MnO_3 using sol-gel technique.* Journal of NeuroQuantology2022, Vol.20, pp.808-812.
20. Haralkar S.J., Kadam R.H., More S.S., Shirsath S.E., Mane M.L., Patil S., Mane D.R. *Intrinsic magnetic, structural and resistivity properties of ferromagnetic $Mn_{0.5}Zn_{0.5}Al_xFe_{2-x}O_4$ nanoparticles.* Mater. Res. Bull. 2013; Vol.48, pp.1189–1196.
21. C. Regmi, B. Joshi, S.K. Ray, G. Gyawali, R.P. Pandey, *Understanding mechanism of photo catalytic microbial decontamination of environmental wastewater,* Front. Chem. 2018, Vol. 6, pp.1–6.
22. Madhukara, N. M.; Bhojya, N. H. S.; Nagaraju, G.; Vinuth, M.; Raja, N. H.; Vinu, K. *Green Synthesis of Zinc Ferrite Nanoparticles in Limonia Acidissima Juice: Characterization and Their Application as Photo catalytic and Antibacterial Activities.* Microchemist. J. 2019, Vol. 146, pp.1227–1235.